Mingqi Liu[1], Antoine Rozel[1], and Taras Gerya[1]

[1]Department of Earth Sciences, ETH Zurich, Sonneggstrasse 5, CH-8092 Zurich

Corresponding author: Mingqi Liu (mingqi.liu@erdw.ethz.ch)

Key Points:

- Fault strength reduction and axial brittle layer thickness are two pivotal factors in controlling faulting patterns and spreading modes
- Axial brittle layer thickness is mainly controlled by spreading rates, hydrothermal circulation, and mantle potential temperature
- Despite grain size reduction being observed at the root of detachment fault, its effect on tectonic patterns is negligible

Abstract

One of the most prominent plate tectonic processes is seafloor spreading. But its formation processes are poorly understood. In this study, we thoroughly address how the brittle-ductile weakening process affects the formation and development of tectonic patterns at spreading centers using 3D magmatic-thermomechanical numerical models. Grain size evolution and brittle/plastic strain weakening are fully coupled into the model. A spectrum of tectonic patterns, from asymmetric long-lived detachment faults in rolling-hinge mode, short-lived detachment faults in flip-flop mode, to symmetric conjugate faults in flip-flop mode are documented in our models. Systematic numerical results indicate that fault strength reduction and axial brittle layer thickness are two pivotal factors in controlling the faulting patterns and spreading modes. Strain weakening induced by localized hydrothermal alteration can lead to the variation of the fault strength reduction. Strong strain weakening with large fault strength reduction results in very asymmetric detachment faults developing in rolling-hinge mode, while weak strain weakening leads to small fault strength reduction, forming conjugate faults. Moreover, the thermal structure beneath the ridge is influenced by spreading rates, hydrothermal circulation, and mantle potential temperature, which in turn controls the thickness of the axial brittle layer and results in variation in tectonic patterns. Further, in order to test a damage mechanism with a physical basis, we investigate grain size reduction at the root of detachment faults. We found that its effect in the formation of detachment faults appears to play a subordinate role compared to brittle/plastic strain weakening of faults.

Plain Language Summary

The global mid-ocean ridge network is a significant system on Earth, where a new oceanic floor is created. As the plates separate, the shape and geometry of a ridge are affected by the spreading rate and accommodated by transform faults. Steep and irregular topography with asymmetric low-angle detachment faults and amagmatic segments is documented in ultraslow-slow spreading ridges while fast-spreading ridges result in symmetric high-angle normal faults combining relatively flat and uniform topography. To better understand the differences, we

employ 3D magmatic-thermomechanical numerical models to explore how the brittle-ductile weakening process affects the formation and development of tectonic patterns at spreading centers. We found that fault strength reduction (controlled by hydrothermal alteration through faults) and axial brittle layer thickness (controlled by spreading rates, hydrothermal circulation, and mantle potential temperature) are two pivotal factors in controlling the faulting patterns and spreading modes. Furthermore, we observed grain size reduction at detachment faults' roots at ultraslow-slow spreading ridges, but its effect on the variation of faulting patterns and spreading modes is negligible. This study provides valuable insights to quantify and explain the deformation process in the global mid-ocean ridge system.

1 Introduction

The process of tectonics and magmatism results in a wide range of fault sizes and orientations at mid-ocean ridges (Buck et al., 2005). In contrast to the symmetric and high-angle normal faults in fast-spreading centers, slow-spreading ridges are characterized by asymmetric, large-offset, and low-angle detachment faults with oceanic core complexes (MacLeod et al., 2011; Sauter et al., 2013). Previous studies suggested that the crucial factor in the seafloor tectonic patterns may be the ratio of magmatically accommodated extension to total plate separation which is mainly controlled by spreading rates (Buck et al., 2005; Olive and Dublanchet, 2020; Liu et al., 2022; Zhou et al., 2022). Low magma supply and thick axial lithosphere in slow-spreading ridges facilitate the formation of detachment faults, while normal faults in axial topographic high spreading centers are very sensitive to fast-spreading rate and thin axial lithosphere with full magma supply. Furthermore, the axial thermal structure reflects a balance between heat advection (e.g., magma ascent and mantle flow) and heat loss (e.g., hydrothermal circulation) (Chen and Morgan, 1990; Morgan and Chen, 1993). The circulation patterns have been characterized by geochemical data and microearthquakes across a wide range of spreading rates (Coogan et al., 2005; deMartin et al., 2007; Grevemeyer et al., 2013; van der Zwan et al., 2017). The hydrothermal circulation depth could reach about 13 km in the ultraslow Southwest Indian Ridge which is much greater than at the Mid-Atlantic Ridge (Tao et al., 2020). In addition, hydrothermal circulation may become more vigorous when the permeability along the fracture increases due to large-offset faults (Escartín et al., 2008; Harding et al., 2017). The heat transfer between the seawater and the hot lithospheric rocks will be enhanced by deep hydrothermal circulation paths, thereby cooling and thickening the axial lithosphere and in turn promoting a low magma supply that favors detachment faulting.

To explain the development of successive detachment faults along the spreading direction, several models have been proposed based on both observations and numerical modeling. The rolling-hinge model, which indicates sequential faulting and the formation of highly asymmetric magma-poor margins of rifted continents, is a typical explanation for the asymmetric architecture and the exhumation of mantle rocks (Buck, 1988). Numerical results from Lavier et al.,

(1999) suggested that the reduction in fault strength plays a crucial role in the fault offset in this model. To interpret symmetric exhumed mantle-derive rocks in the Southwest Indian Ridge, Sauter et al., (2013) proposed the flip-flop model that asymmetric detachment faults develop through successive polarity changes. This may be caused by an insufficient magma supply and the enhanced hydrothermal circulation and alteration near the faults. Furthermore, the seismic observations along the Iberia-Newfoundland and Australia-Antarctica margins revealed the development of multiple out-of-sequence asymmetric detachment faults. The jump deformation model was proposed by Gillard et al., (2016) to account for the transition from fault-controlled (the early stage of exhumation at rift margins) to magma-controlled (the localized stages at stable spreading centers) strain accommodation. This transition may be induced by variations in the spreading rates, brittle layer thickness, and magma supply (Huismans and Beaumont, 2003; Gillard et al., 2016). But the dynamic development and rheological mechanism of detachment faulting patterns along the spreading direction are not well-constrained and need further investigation.

Previous studies have shown that strain weakening impacts faulting patterns (Huismans and Beaumont, 2002, 2003; Buck et al., 2005). In the absence of stain weakening, extension is symmetric. In contrast, increasing strain weakening through reducing the internal frictional coefficient results in asymmetric extension at the lithospheric scale or asymmetric at the crustal scale while maintaining the symmetry of the mantle (Huismans and Beaumont, 2002, 2003). The frictional plastic and ductile layers are critical factors in controlling different styles. Furthermore, the fast strain weakening, sudden loss of cohesion, produces small-offset normal faults similar to those seen in the axial-high fast-spreading centers. Slower strain weakening cause large-offset detachment faults consistent with slow-spreading centers. These large-offset detachments could root into a brittle-ductile transition region (Olive et al., 2010), which provides channels for fluid-rock reactions (e.g., serpentinization) (e.g., Andreani et al., 2014; Bach et al., 2004, 2006; Beard et al., 2009; Boschi et al., 2006, 2013; Klein et al., 2009; Maffione et al., 2014; Mével, 2003; Plümper et al., 2012, 2014; Schroeder et al., 2002). As a result, oceanic lithospheric strength around spreading centers significantly decreases (MacLeod et al., 2002), and plastic strain localization is markedly enhanced.

Though explaining the formation of detachment faults, strain weakening only phenomenologically produces the observed strain localization in nature. In contrast to relatively well-documented localization in the brittle layer (Paterson, 2005), the processes of strain localization in the ductile regime (or mylonitization) are relatively weakly constrained (e.g., Poirier, 1980). Strain localization in the tectonically driven oceanic lithosphere deformation is controlled by frictional faults under low pressure and temperature conditions and by mylonitic ductile shear zones with a lack of crystal-preferred orientation under high pressure and temperature conditions. The process in mylonitic ductile shear zones may be related to a sudden loss of strength caused by deformation-driven grain size reduction. It leads possibly to grain-size-sensitive diffusion creep competing

with dislocation creep to become the dominant weakening mechanism (Poirier, 1980). This hypothesis has been supported by numerical and experimental studies as well as natural observation of grain size reduction in strongly deformed lithospheric mantle shear zones (Bercovici and Ricard, 2012; Bickert et al., 2020, 2021; Rozel et al., 2011; Vissers et al., 1995).

Thus, in this study, we thoroughly investigate how the brittle-ductile weakening process affects the formation and development of tectonic patterns at spreading centers using 3D magmatic-thermomechanical numerical models. Brittle/plastic strain weakening and grain size evolution are fully coupled into the model. Strain weakening intensity, spreading rate, mantle potential temperature, and grain damage are tested to reproduce the essential features of tectonic patterns. A wide span of faulting patterns and development of successive faults, from asymmetric long-lived detachment faults to symmetric conjugate faults and from rolling-hinge mode to flip-flop mode, are documented in our numerical results. We provide detailed parameter sets, controlling different tectonic patterns at spreading ridges.

2 Numerical Methods

Based on the code I3ELVIS, we employ 3D magmatic-thermomechanical numerical models. The specific version of the code is modified from Liu et al., (2022). The oceanic spreading process is implemented through four simplified key processes (Gerya, 2013; Liu et al., 2022 and references therein). To simulate the hydrothermal circulation process near spreading centers, an enhanced thermal conductivity of the crust is implemented:

$$\kappa_{\text{eff}} = \kappa + \kappa_0(\text{Nu}-1)exp\left(A\left(2 - min\left(1, \frac{T}{T_{\text{max}}}\right) - min\left(1, \frac{y}{y_{\text{max}}}\right)\right)\right), (1)$$

κ is the thermal conductivity of dry rocks $\left[\kappa = 1.18 + \frac{474}{T+77}\right.$ for the crust and $\kappa = 0.73 + \frac{1293}{T+77}$ for the mantle$\left.\right]$, $\kappa_0 = 3\ W/(m \bullet K)$ is the reference thermal conductivity, and Nu is the assumed Nusselt number. T (℃) is temperature. y $(km)$is depth. The maximum temperature(T_{max}) and the maximum depth (y_{max}) of hydrothermal circulation are 600 ℃ and 6 km, respectively. A is a smoothing factor and 0.75 is used in this study.

The effective strength of the oceanic lithospheric plate is computed using viscoplastic rheology. The viscous and brittle/plastic rheology properties are shown in Table S1. In the brittle/plastic region, fracture-related strain weakening is implemented through the upper (φ_0) and lower (φ_1) limits of frictional coefficient and the upper (γ_0) and lower (γ_1) strain limits. In the ductile part, the effective ductile viscosity following a composite law is calculated by harmonic averaging of both dislocation and diffusion creeps. Grain size is not considered in the crustal material, while the process of both grain damage and grain growth is employed in the mantle rocks. A constant low value limits the viscosity of partially molten

crustal and mantle rocks. The minimal value between the plastic and ductile rheology is defined as the final effective viscosity: $\eta_{\text{eff}} = min(\eta_{\text{plastic}}, \eta_{\text{ductile}})$, further limited by the cut-off values of $[10^{18}, 10^{24}]$ Pa$\bullet s$. The detailed numerical method and grain size evolution process could be obtained from the Supporting information and Liu et al., (2022).

Due to the uncertainty of damage fraction f_I, the following two different temperature-dependent formulas are explored in this study: (a) an exponential form (Rozel et al., 2011); (b) a power law form (Schierjott et al., 2020).

$$f_I = f_0 \exp\left(-2\left(\frac{T}{1000}\right)^{2.9} + 2\right), (2a)$$

$$f_I = f_{\text{top}}\left(\frac{f_{\text{bot}}}{f_{\text{top}}}\right)^{\frac{T-T_{\text{surf}}}{T_{\text{CMB}}-T_{\text{surf}}}}, (2b)$$

where f_0 in Equation $2a$, the interface damage at 1000 K, is a constant. Three different values ($1e-1$, $1e-2$, and $1e-3$) are tested. For the formula in Equation $2b$, $T_{\text{surf}} = 273$ K is the surface temperature, and $T_{\text{CMB}} = 3727K$ is the temperature of the core-mantle boundary. The range of damage friction is limited by f_{top} and f_{bot}. A large f_{bot} results in a strong damage fraction. In this study, $f_{\text{top}} = 1e-2$, the maximum damage friction, is a fixed value. f_{bot}, the minimum damage friction, is varied from $1e-2$ to $1e-9$.

2.1 Initial model setup

Following the setting in Liu et al., (2022), the initial model mimics how oceanic spreading evolves along symmetric and homogeneous spreading centers (Figure 1). The model domain is $202 \times 202 \times 98$ km with a very high resolution (0.5 km) and about 130 million random markers. In order to obtain the seafloor topography, an initial 10-km "sticky air" layer (air and water) is implemented above the oceanic plate. The symmetric thermal configuration is implemented using the half-space cooling model (10 Myr-old oceanic plates in both left and right boundaries and the spreading ridge in the center). The top boundary maintains a constant temperature (273 K). Different temperatures are implemented in the bottom boundary to examine the effect of mantle potential temperature. The constant spreading velocities are imposed in both left and right boundaries along the x-direction ($v_{\text{spreading}} = v_{\text{left}} + (-v_{\text{right}})$, where $v_{\text{left}} = -v_{\text{right}}$). To guarantee the mass conversion in the model domain, influx velocities are implemented through the upper (v_{top}) and lower (v_{bottom}) boundaries along the z-direction (Gerya, 2013; Liu et al., 2022).

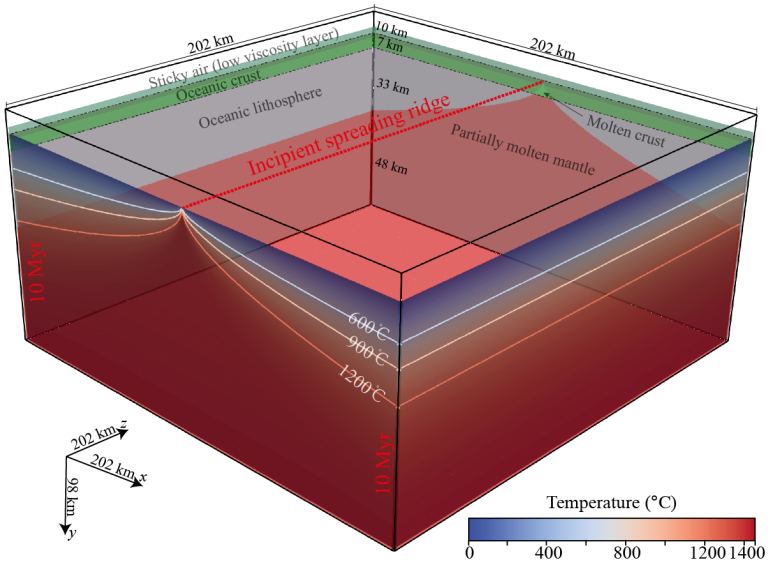

Figure 1. Initial model setup. Thermal distribution (front and right sides) and compositional distribution (left and back sides). The dashed red line on the top marks the incipient spreading ridge. Colorful lines on the front and right sides show the isotherms.

3 Numerical results

As shown in Table 1, a large number of models with four sets of parameters are run to investigate their effects on the faulting patterns at spreading centers and the development of successive faults along the spreading direction and explore their formation mechanism. (1) Variable strain weakening intensities ranging from 0.6 to 0 are implemented. (2) Full spreading rates of 5 to 80 mm/yr are imposed to simulate incipient ultraslow- to fast-spreading ridges, and varying bottom temperatures are configured to model different mantle potential temperatures. (3) Variable Nusselt numbers are implemented to simulate hydrothermal circulation intensity at spreading centers. (4) Grain size growth and damage parameters are also implemented to explore the effect of grain size on the geometry of the flow. Through these models, a wide span of faulting patterns and development of successive faults, from asymmetric long-lived detachment faults to symmetric conjugate faults and from rolling-hinge to flip-flop mode, are documented in our models (Figure 2). The following sections show the effects of most tested parameters on tectonic patterns (Figure 3-6).

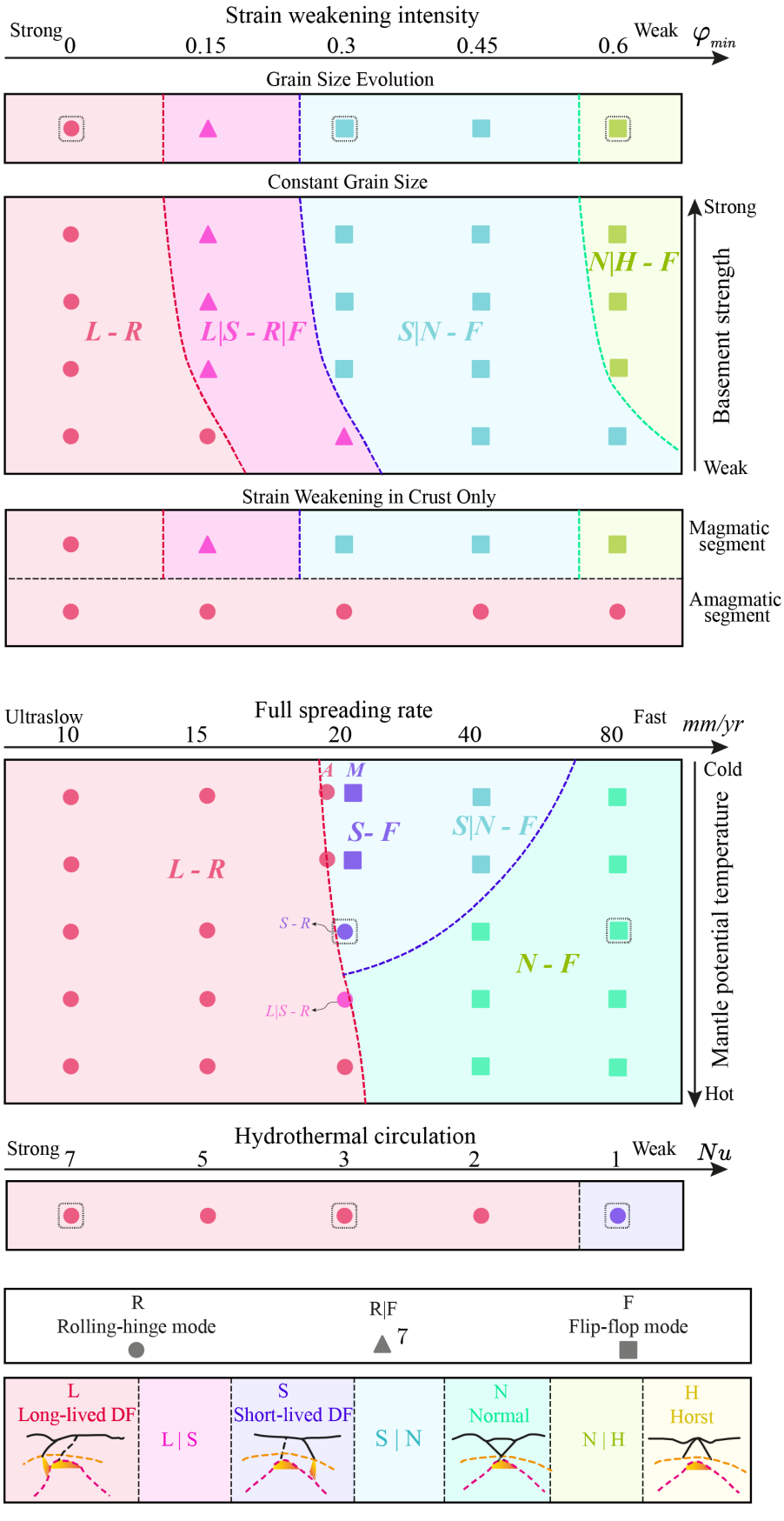
Strain weakening intensity
Strong
0
0.15
0.3
0.45
0.6
Weak
φ_{min}
Grain Size Evolution
Constant Grain Size
L - R
L|S - R|F
S|N - F
N|H - F
Strong
Basement strength
Weak
Strain Weakening in Crust Only
Magmatic segment
Amagmatic segment
Full spreading rate
Ultraslow
10
15
20
40
80
Fast
mm/yr
A
M
S- F
S|N - F
L - R
S - R
L|S - R
N - F
Cold
Mantle potential temperature
Hot
Hydrothermal circulation
Strong
7
5
3
2
1
Weak
Nu
R
Rolling-hinge mode
R|F
7
F
Flip-flop mode
L
Long-lived DF
L | S
S
Short-lived DF
S | N
N
Normal
N | H
H
Horst

Figure 2. Summary of numerical results. Results with different dominated faulting patterns and development modes of successive faults are clarified. Models with variable strain weakening intensity are shown in the top three panels. In the first panel, models implemented by different initial grain sizes were run with grain size evolution, and models with constant grain size were run in the second panel. In the third panel, variable strain weakening intensities are only implemented in the oceanic crust. In the fourth panel, models with variable spreading rates and mantle potential temperatures were run. In the last panel, we show the effects of hydrothermal circulation. Symbols (circle, triangle, and square) represent different development modes of successive faults along the spreading direction. Colors mark faulting patterns at the spreading centers. Dashed squares denote the representative evolutions in Figure 3.

3.1 Effects of strain weakening intensity

Models with variable strain weakening intensity are shown in Figure 3a. For each strain weakening intensity, several quantities are shown in 5 subplots: (top) the strain rate in the 3D volume, (bottom left) a horizontal slice of the domain at 20 km depth showing the second invariant of the strain rate, (bottom right, top plot) a vertical slice, located at the red line on the 3D and horizontal plots, showing the strain rate, (bottom right, center plot) the grain size, (bottom right, bottom plot) the dominating rheology. All bottom right subplots show sea level, topography, brittle-ductile transition, and melt boundary.

Similar to a recent study by Liu et al., (2022), magmatic and amagmatic segments can alternate along spreading centers, depending on various parameters. This is particularly visible in the model with strong strain weakening intensity. In the horizontal slice, one can see wide regions of large deformation (yellow/orange) alternating with very localized segments (dark blue/green surrounded by thin orange/red segments). The localized segments are the amagmatic portions where the mantle material is exhumed. The yellow/reddish diffuse segments are the magmatic sections where magma rises near the surface through detachment faults, forming a new oceanic crust. In amagmatic segments (through which goes our vertical slice), grain damage occurs at the interface of brittle-ductile transition where the deviatoric stress magnitude reaches the peak. Mantle rocks with small grain size exhume through detachment faults as can be seen in the grain size subplot (i.e., grey regions are crustal rocks, and non-grey regions are mantle rocks). Small grain size at the root of detachment faults in the ductile region leads to grain-size sensitive diffusion creep which may reduce the strength and enhance the strain localization there. Owing to the strength reduction in the fault from both strain weakening and grain damage, the fault continues to slip and forms long-lived detachment faults with large offset, resulting in very asymmetric spreading centers and smooth topography at the seafloor. In addition, the next fault forms with the same dip (rolling-hinge mode) in the footwall after the offset reaches about 30 km. With the reduction of strain weakening intensity, strength reduction of faults drops, resulting in the decrease of fault offset. Short-lived detachment faults with small offset form in

the intermediate strain weakening intensity and their polarities change intermittently (flip-flop mode) and are accommodated through normal faults. Spreading centers become relatively symmetric and topography at the seafloor undulates. In the model without strain weakening, high-angle normal/horst faults with extremely small offset and successive polarity changes are observed. Grain damage is mainly observed at the root of faults near the brittle-ductile transition region and then moves away from the spreading centers. The spreading ridge is low and symmetric and topography strongly undulates when compared with models with strong strain weakening intensity.

Therefore, the strain weakening intensity plays a key role in the faulting patterns at spreading centers and the development of successive faults along the spreading direction. With the reduction of strain weakening intensity, the fault offset gradually decreases, resulting in the variation from long-lived detachment faults, short-lived detachment faults, to high-angle normal/horst faults. The spreading mode changes from very asymmetric rolling-hinge mode to symmetric flip-flop mode, spreading centers vary from strongly curved to straight, and topography at the seafloor also changes from relatively flat to strongly undulated. Furthermore, due to the hot thermal structure, a thin brittle layer, and no grain damage at the root of detachment fault in magmatic segments, the fault offset is rather small, and magmatic segments are accommodated by adjacent amagmatic segments (Liu et al., 2022). This phenomenon is also documented by models with a variety of strain weakening only in the crust, in which strong magmatic segments are accommodated by weak amagmatic segments. However, regardless of magmatic or amagmatic segments, similar tectonic patterns are observed when the same strain weakening intensity is implemented.

3.2 Effects of spreading rate and mantle potential temperature

In contrast to strain weakening intensity, the prominent features induced by spreading rate and mantle potential temperature changes are the variation of the thermal configuration under the ridge and the brittle layer thickness at spreading centers (Figure 3b).

At ultraslow (5 mm/yr) spreading centers, cold thermal structure, and very small magma supply cause spare and narrow magmatic segments, very thick brittle layer, and long-lived detachment faulting developing through rolling-hinge mode. Grain damage at the deep root of long-lived detachment faults leads to grain-size sensitive diffusion creep in the ductile regime. With the increasing spreading rate, thermal structure, and magma supply at spreading centers increase, leading to a rapid reduction of brittle layer thickness and widening of magmatic segments.

At slow (20 mm/yr) spreading centers, only several narrow amagmatic segments are documented and the brittle layer thickness is much thinner than that in ultraslow spreading centers. The fault offset sharply reduces, resulting in short-lived detachment faults. Owing to the rolling-hinge mode along the spreading direction, the topography is relatively flat. In addition, lowering mantle potential

temperature can cause a colder thermal structure and slightly thicker brittle layer thickness at spreading centers (Liu et al., 2022). In models with low mantle potential temperature, a relatively thick brittle layer in amagmatic segments induces long-lived detachment faults developing through rolling-hinge mode. On the other side of the spectrum, a thin brittle layer thickness in magmatic segments produces short-lived detachment faults spreading through flip-flop mode (the fourth panel in Figure 2).

In contrast, in models with high mantle potential temperature, the thermal structure produces sufficient magma beneath spreading centers, resulting in a full magmatic segment with thick new oceanic crust and a thin brittle layer (Liu et al., 2022). But the very weak ductile regime induced by the high temperature promotes the formation of long-lived detachment faults and the evolution of the rolling-hinge mode. Continuously increasing spreading rates lead to common high-angle normal faults developing in flip-flop mode. And the mantle potential temperature can slightly influence the variation of faulting patterns (the fourth panel in Figure 2).

At the fast (80 mm/yr) spreading centers, hot thermal structure leads to an extremely thin brittle layer, around 1.5 km, beneath spreading centers, which develops through symmetric normal faults in flip-flop mode and is very straight with flat topography. Thus, spreading rates has an impact on the brittle layer thickness and can cause the faulting patterns to vary from long-lived detachment faults in rolling-hinge mode at ultraslow-spreading centers, short-lived detachment faults in rolling-hinge and/or flip-flop mode at slow-spreading centers, to high-angle normal faults in flip-flop mode at fast-spreading centers. Mantle potential temperature can also change the tectonic patterns, but its effect is mostly visible in transition regimes at slow-spreading centers, as shown in the fourth panel of Figure 2.

3.3 Effects of hydrothermal circulation

Hydrothermal circulation strongly affects the thermal structure of the lithosphere and brittle layer thickness at spreading centers. To explore its effects, enhanced thermal conductivity near the surface is implemented in this study to simulate hydrothermal circulation at spreading centers (Figure 3c). Numerical results show that stronger hydrothermal circulation near spreading centers facilitates heat transfer, cooling the thermal structure and reducing magma supply and thereby increasing the thickness of the axial brittle layer.

In the models with strong hydrothermal circulation ($Nu = 7$), a cold and thick axial lithosphere leads to sparse and narrow magmatic segments, a thick brittle layer, and long-detachment faults in rolling-hinge mode. Large fault offset produces very asymmetric spreading centers, which is consistent with the observation in poor-magma rift margins (Gillard et al., 2016). With the decreasing hydrothermal circulation intensity, reducing heat loss produces a hot axial thermal structure with more magma supply, resulting in wide magmatic segments and thin brittle layer thickness.

In the model with intermediate hydrothermal circulation ($Nu = 3$), the thermal structure is warmer at spreading centers, resulting in wider magmatic segments, a thinner axial brittle layer thickness, and a smaller fault offset. Yet, the thinned axial brittle layer still leads to the production of long-lived detachment faults in rolling-hinge mode.

Finally, in the model without enhanced hydrothermal circulation ($Nu = 1$), owing to extremely small heat loss, the axial lithosphere is very hot with sufficient magma supply. A full magma segment is documented. In addition, the thin brittle layer leads to very short-lived detachment faults developing in rolling-hinge mode, which may be mainly related to the strong strain weakening (Table 1).

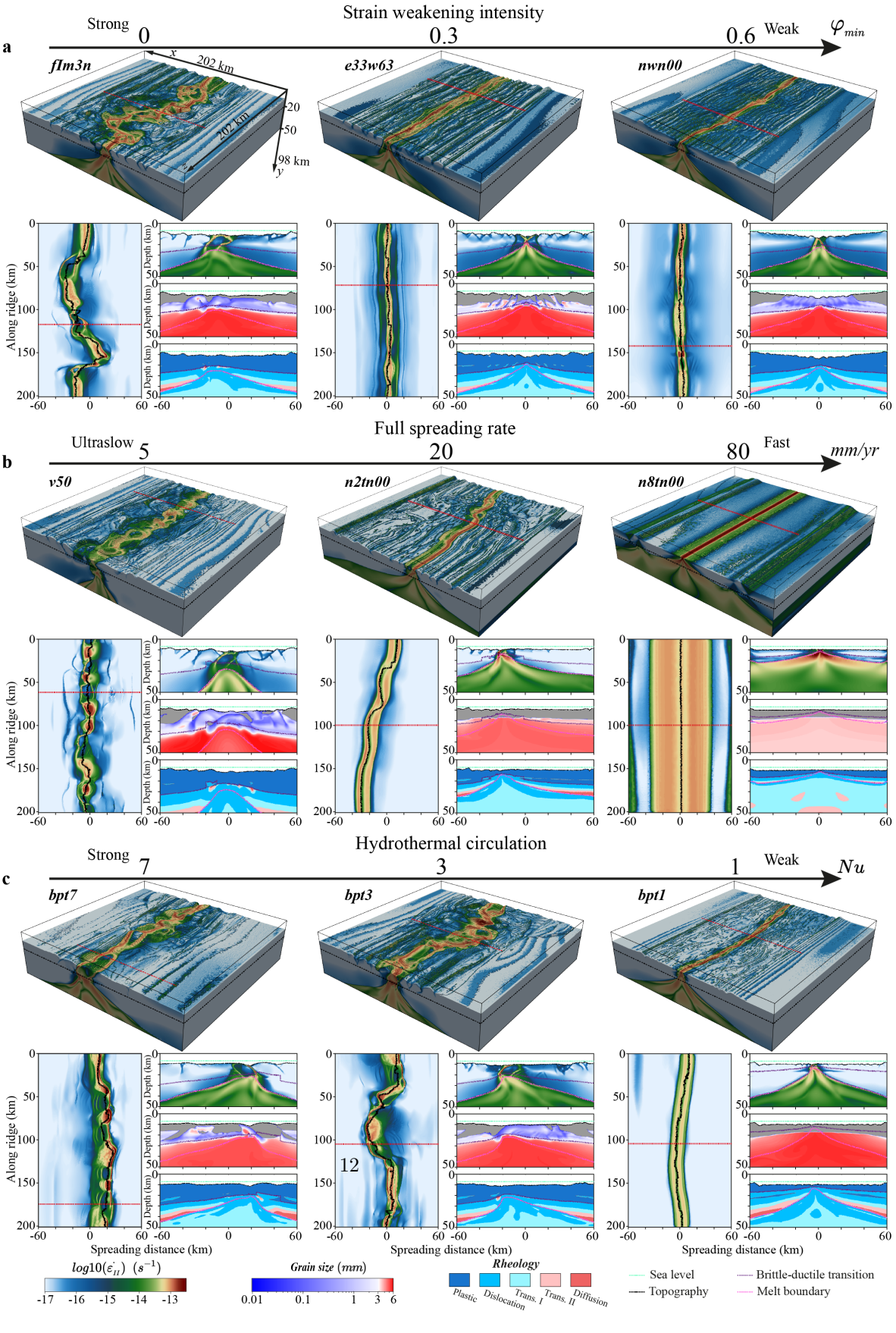
a
Strain weakening intensity
Strong
0
0.3
0.6
Weak
φ_{min}
flm3n
e33w63
nwn00
202 km
202 km
98 km
20
50
x
y
b
Full spreading rate
Ultraslow
5
20
80
Fast
mm/yr
v50
n2tn00
n8tn00
c
Hydrothermal circulation
Strong
7
3
1
Weak
Nu
bpt7
bpt3
bpt1
12
Along ridge (km)
Depth (km)
Spreading distance (km)
$log10(\dot{\varepsilon}_{II})$ (s^{-1})
-17 -16 -15 -14 -13
Grain size (mm)
0.01 0.1 1 3 6
Rheology
Plastic
Dislocation
Trans. I
Trans. II
Diffusion
Sea level
Topography
Brittle-ductile transition
Melt boundary

Figure 3. Representative numerical results at about 120 km full spreading distance. Model parameters are given in Table 2. Effects of strain weakening intensity (a), full spreading rate (b), and hydrothermal circulation at spreading centers (c) are presented. In each model, a 3D plot with the second strain rate invariant is shown at the top. Below the 3D plot, a horizontal slice with the second stain rate invariant at a depth of 20 km is shown. The dashed black line marks spreading centers at the seafloor and the dashed red line represents the location of vertical profiles in the right panel. The second strain rate invariant, grain size distribution, and rheological mechanism are shown in vertical profiles. The initial spreading center location is at 0 km. Along ridge direction corresponds to the z axis.

3.4 Effects of self-consistent grain size evolution

Previous studies have proposed that damage may lead to grain-size sensitive diffusion creep and reduce the plate strength (Bercovici and Ricard, 2012; Bickert et al., 2021), but their effects on tectonic patterns are not well constrained. Here, through self-consistent grain size evolution, we systematically investigate the influence of grain damage and diffusion creep in faulting patterns and development modes of successive faults. Models with grain size evolution and with constant grain size were compared to explore the effect of damage on tectonic patterns. Parameters include variable initial grain size (0.01, 0.1, 1, and 6 mm), grain size reduction fraction (exponential formulas and power-law formulas), and grain-size sensitive diffusion creep prefactor (from 0.01 to 100 times larger than a chosen reference case).

3.4.1 Effects of grain size evolution on the tectonic pattern

Models with implemented grain damage and with constant grain size are compared in Figure 4 and numerical results in these two kinds of models share similar tectonic patterns except for models with very small initial grain size (0.01 mm). For grain damage models, even though variable initial grain sizes are implemented, small grain sizes are observed along detachment faults in amagmatic segments. Relatively uniform grain sizes (3-6 mm) were formed in the ductile regime over about 12-Myr evolution in both magmatic and amagmatic segments, which may be mainly induced by the balance between grain growth rate and grain damage rate (Figure 5) at stable spreading centers. Dynamic recrystallization at the root of detachment faults in amagmatic segments leads to grain-size sensitive diffusion creep. Long-lived detachment faults formed and developed through both rolling-hinge mode and flip-flop mode. However, in the model with a very small initial grain size (0.01 mm), owing to the slightly smaller grain size (3-4 mm) in the ductile regime, the fault offset is a little larger and the topography is slightly flatter than in other models.

In models with constant grain size, the rheological mechanism strongly depends on the imposed grain size. In the model with large grain size, dislocation creep dominates in the ductile regime and no grain-size sensitive diffusion creep ever appeared at the root of detachment faults. Long-lived detachment faults de-

veloped through both rolling-hinge mode and flip-flop mode. At intermediate grain size, the rheological mechanism at ductile regime changes from dislocation creep dominant to diffusion creep dominant. The fault strength reduces and fault offset increases at amagmatic segments and the development mode of successive detachment remains identical. Finally, in the model with a very small initial grain size (0.01 mm) diffusion creep dominates, and the extremely weak mantle leads to vigorous convection in the ductile regime. Fault offsets are then larger and detachment faults develop only through rolling-hinge mode. Comparing these two sets of models (the first two panels in Figure 2), we can see that although grain damage at the root of detachment faults can facilitate the strength reduction and increase the fault offset, its role in tectonic patterns is very small compared to the effect of strain weakening.

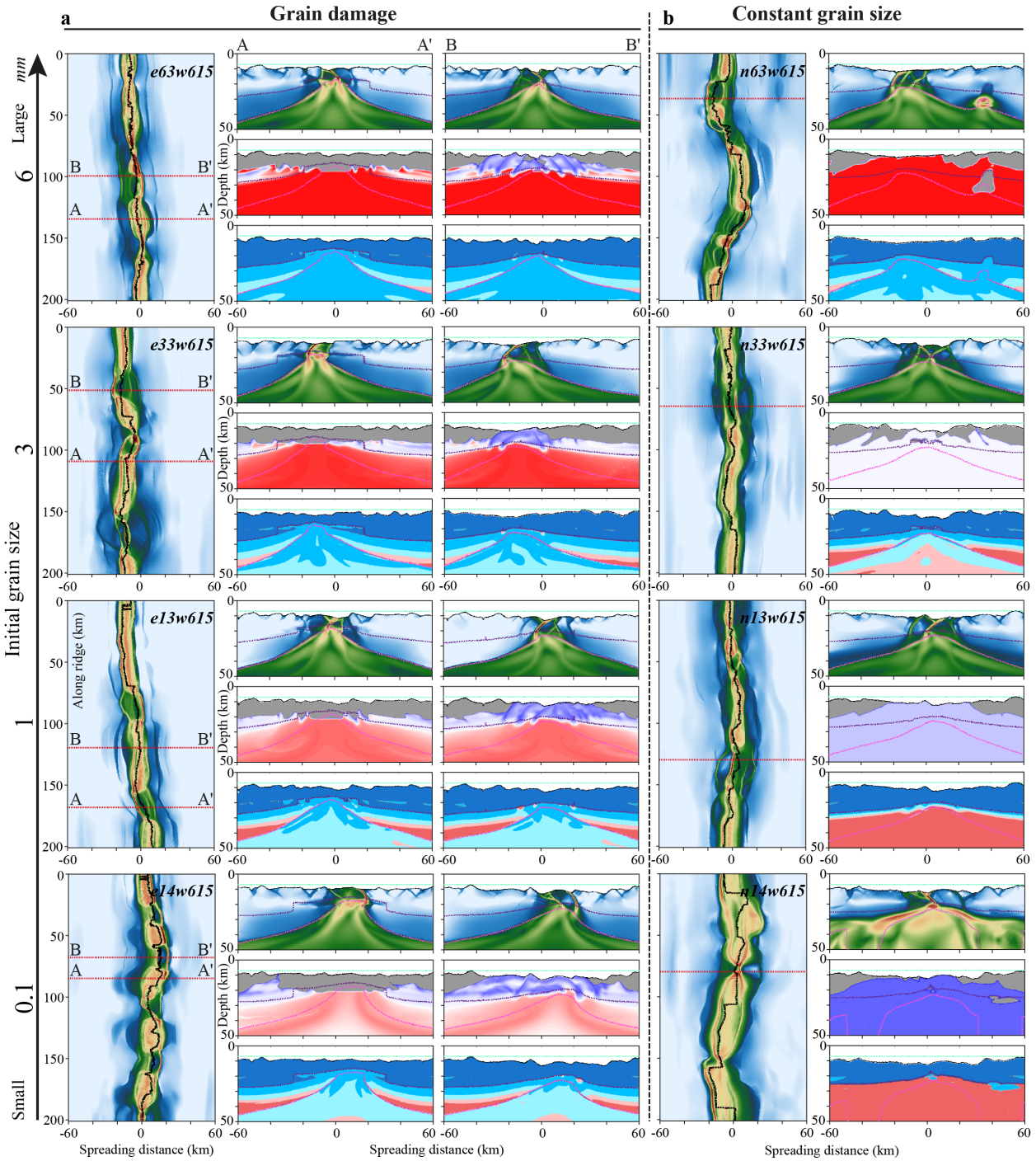

Figure 4. Numerical results with variable initial grain size at about 120 km

spreading distance. $\varphi_{\min} = 0.15$ is implemented in these models. a, models considering grain size evolution. b, models employing a constant grain size. In subplots: a horizontal slice at 20 km depth shows the second strain rate invariant (left). Vertical sections are shown with both magmatic segments (middle) and amagmatic segments for models with grain size evolution. Only amagmatic segments are represented for models with constant grain size. Color codes are the same as in Figure 3.

3.4.2 Varying the intensity of dynamic recrystallization

To systematically explore the effect of dynamic recrystallization on tectonic patterns, two sets of damage fraction intensities were tested and reported in Figure 5. See Equations 2a,b and Equation 15c (in the Supporting information) for the definition and use of the damage fraction f_I. This fraction represents the amount of mechanical work redirected in the grain size reduction term, instead of generating shear heating. Our results show that f_I is directly related to the rheological mechanism at the root of detachment faults. For both damage fraction formulations, we can see that using a large damage fraction produces stronger grain damage at the root of detachment faults. This makes diffusion creep more prominent and therefore enhances strength reduction. When the damage fraction is large, we observe that dynamics recrystallization limits the grain size in the entire ductile region of the models. At a lower damage fraction, grain growth tends to balance dynamic recrystallization, resulting in relatively homogeneous and large grain size in the high temperature region, probably induced by small damage fraction in high temperature in both formulas.

In the brittle layer, we observe that the grain size of uplifted mantle rocks is strongly influenced by the damage fraction at intermediate or high temperature. Indeed, the absolute value of the parameter f_I in the PT conditions of the root of the detachment fault has a stronger influence than grain growth in the colder regions. Thus, for a large parameter f_I at intermediate/high temperature, the grain size in uplifted rocks remains small despite grain growth being active. Furthermore, although variable damage fractions are significant for grain size distribution and reduce the strength of faults and solid mantle in the ductile regime, long-lived detachment faults formed in a similar manner and developed through rolling-hinge mode. The effect of grain size evolution on the geometry of tectonic patterns seems therefore negligible.

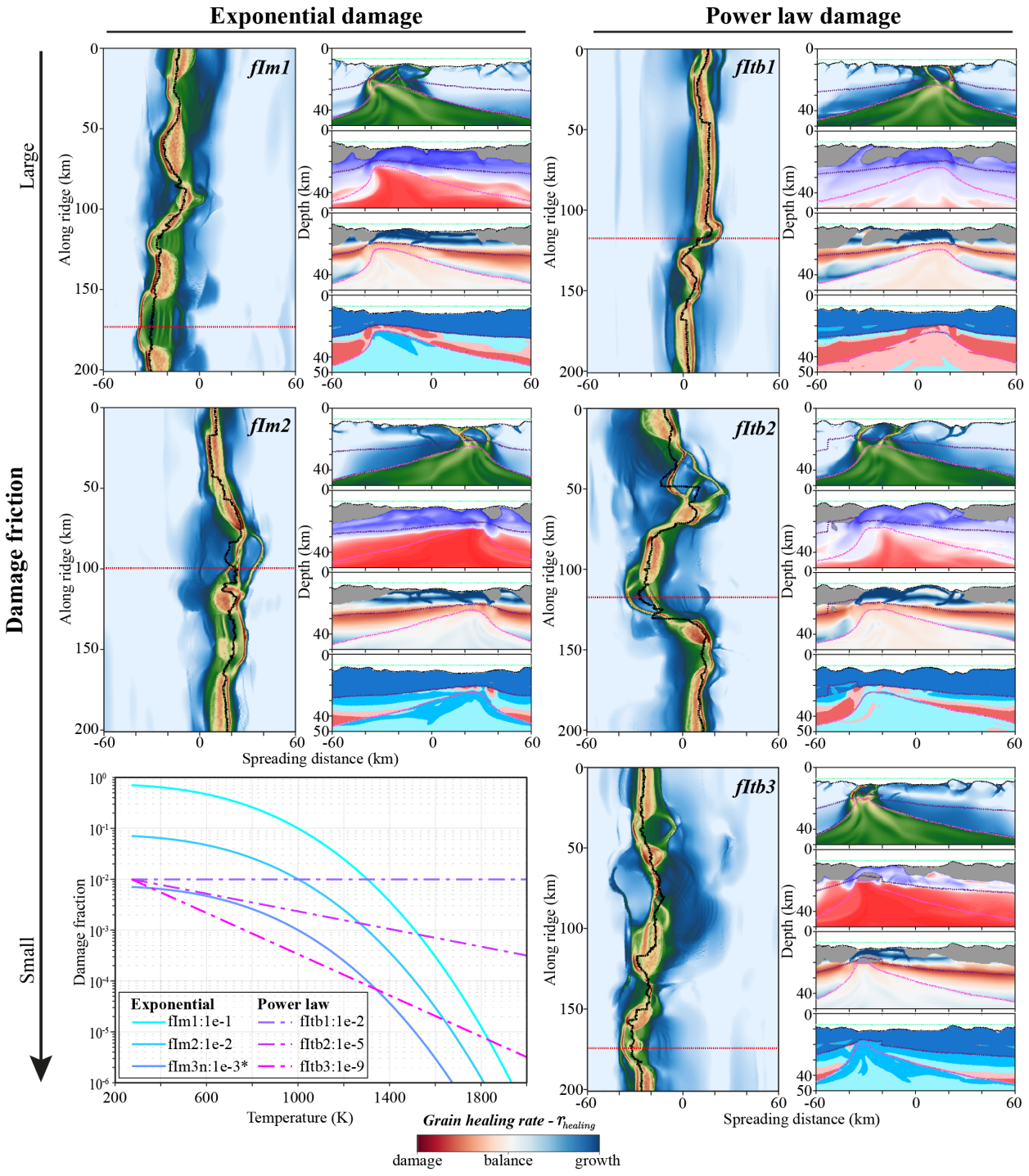
Exponential damage
Power law damage
Damage friction
Large
Small
fIm1
fIm2
fIm3
fItb1
fItb2
fItb3
Along ridge (km)
Depth (km)
Spreading distance (km)
Damage fraction
Temperature (K)
Exponential
fIm1:1e-1
fIm2:1e-2
fIm3n:1e-3*
Power law
fItb1:1e-2
fItb2:1e-5
fItb3:1e-9
Grain healing rate - $r_{healing}$
damage
balance
growth

Figure 5. Model results considering different formalisms and absolute values of the damage fractions. Two sets of damage fraction formulas are presented at the bottom left-hand corner. * marks the reference model. Numerical results are shown at about 120 km spreading distance. The horizontal slice marks the second invariant of the strain rate tensor at a depth of 20 km. Vertical profiles show (from top to bottom) the second invariant of the strain rate tensor, the grain size, the grain growth to grain damage difference, and the dominant rheological mechanism.

3.4.3 Effects of the diffusion creep prefactor

The effects of grain size evolution, initial grain size, and damage fraction on tectonic patterns very found to be negligible. Additionally, we now investigate the effect of grain-size sensitive diffusion creep through changing its prefactor (A_{df} in Equation 11 of Supporting information and Table S1). We now employ three different grain-size sensitive diffusion creep prefactors (from 0.01 to 100 times), as shown in Figure 6. A small prefactor (0.01 times the reference value) leads to a dislocation creep dominant ductile regime as η_{ds} is smaller than η_{df}. When using a large prefactor, η_{df} decreases and the rheology is dominated by diffusion creep. Although we do observe the activation of these different rheological mechanisms, grain damage along detachment faults at amagmatic segments is still observed in all models which share similar tectonic patterns – long-lived detachment faults developing in rolling-hinge mode. This may be related to the fact that a low viscosity for the partially molten crustal and mantle rocks was assumed in our models (Gerya, 2013) which leads to a rather small reduction in strength in the solid lithospheric mantle above the partial melting region. Due to the same damage fraction in these models, a relatively uniform and consistent grain size distribution in the ductile regime is seen in all models. Similar to the model with constant grain size (1 mm), although grain-size sensitive diffusion creep dominants when using a large prefactor (100 times), the rheology is not aggressive enough to induce a very weak solid lithospheric mantle (as in the model with a very small grain size in Figure 4), resulting in similar tectonic patterns than what is seen in other models (Figure 6). Thus, the effect of grain-size sensitive diffusion creep in tectonic patterns at spreading centers is still negligible.

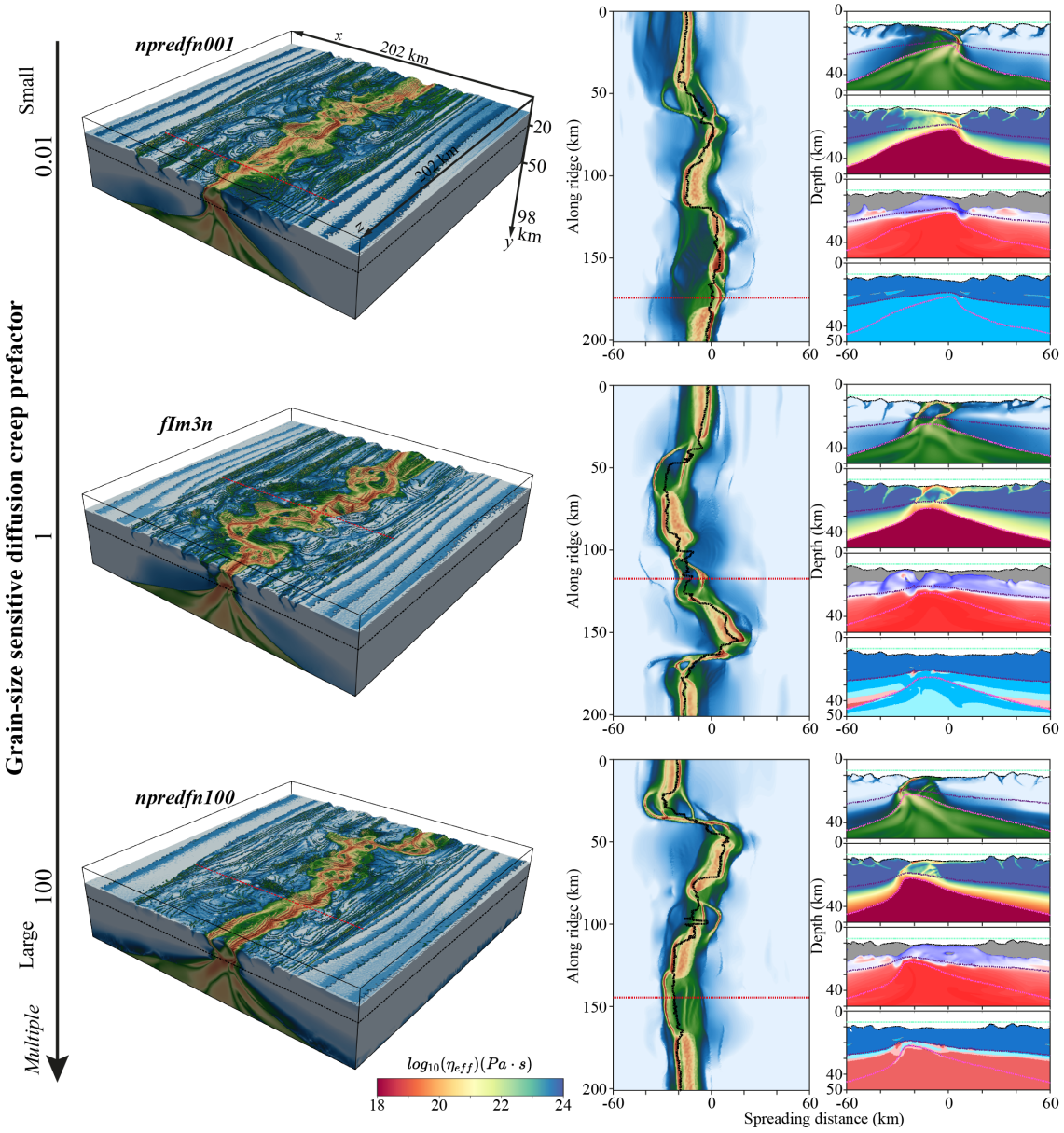

Figure 6. Models with different diffusion creep prefactors (0.01, 1, and 100). Except for the new panel of effective viscosity, other color codes are the same in Figure 3.

4 Discussion

A spectrum of tectonic patterns, from asymmetric long-lived detachment faults in rolling-hinge mode to symmetric conjugate faults in flip-flop mode, are doc-

umented in our models. We observe that the axial brittle thickness and the fault strength play an essential role in forming the faulting patterns and spreading modes at spreading centers. We summarize here the variation of faulting patterns and spreading modes, discuss pivotal factors to control the tectonic patterns, and explore why the effect of grain damage is insignificant. Furthermore, we suggest a set of spreading mechanisms that can explain the development of successive detachment faults along the spreading direction and compare them with natural observations.

4.1 Transitions in faulting patterns and spreading modes

As shown in Figure 7, the intensity of strain weakening, the full spreading rate, and the magnitude of hydrothermal circulation are pivotal factors that control the variations of faulting patterns and spreading modes. Interestingly, Figure 7 shows a strong correlation between the tectonic patterns and the thickness of the brittle layer.

Strain weakening intensity (which may be induced by hydrothermal fluids and serpentinization) can reduce the fault strength (Escartín et al., 2001) and favor fault slip (Lavier et al., et al., 1999). When a strong strain weakening is considered, fault strength is considerably reduced. This leads to the formation of long-lived and very asymmetric detachment faults in rolling-hinge mode, regardless of whether segments are magmatic or amagmatic. When strain weakening intensity is decreased, fault strength reduces and new faults tend to form, as opposed to the persistence of the extensional slip (Lavier et al., 1999). This results in the decrease of fault offsets and the formation of symmetric conjugate faults. Consequently, spreading modes transit from rolling-hinge to flip-flop. To compare with natural observations at spreading centers (Cannat et al., 2019), we implement strong strain weakening intensity in mantle rocks which may be induced by localized hydrothermal alteration of faults (Escartín et al., 2001) and variable strain weakening intensities in crustal rocks. Consistent with observations, long-lived asymmetric detachment faults are observed in amagmatic segments and symmetric conjugate faults are observed in the models with weak strain weakening, and fault strength reduction (Figure 2). In addition, the coupling degree between the brittle layer and the underlying ductile layer can also influence the spreading mode. Weak coupling in models with very small constant grain size (Figure 4) or high mantle potential temperature (Liu et al., 2022) tends to form asymmetric faults developing in rolling-hinge mode. This is consistent with previous numerical results (Huismans and Beaumont, 2002, 2003).

As for the axial brittle layer, we observe that it can affect the formation of new faults and lead to the transition from detachment to conjugate faults. A thick axial brittle layer prevents the formation of new faults and facilitates fault slip, resulting in asymmetric long-lived detachment faults. New faults are prone to form when axial brittle layers are thin, which leads to symmetric conjugate faults (Sibrant et al., 2018; Olive and Dublanchet, 2020). In our models with strong strain weakening, detachment faults form with a thick axial

brittle layer (> 3 km) and conjugate faults only form in a thin brittle layer (< 2km). Spreading rates and hydrothermal circulation play a significant role in controlling the axial brittle layer thickness. Ultraslow and slow-spreading rate and strong hydrothermal circulation enhance the heat transfer and thicken the axial brittle layer thickness, which favors detachment faulting. This is confirmed by the numerical results (Olive and Dublanchet, 2020; Liu et al., 2022) and the observation in magma-poor rifted margins (Gillard et al., 2019) where thick brittle layer and low magma supply results in very asymmetric detachment patterns at the early stage.

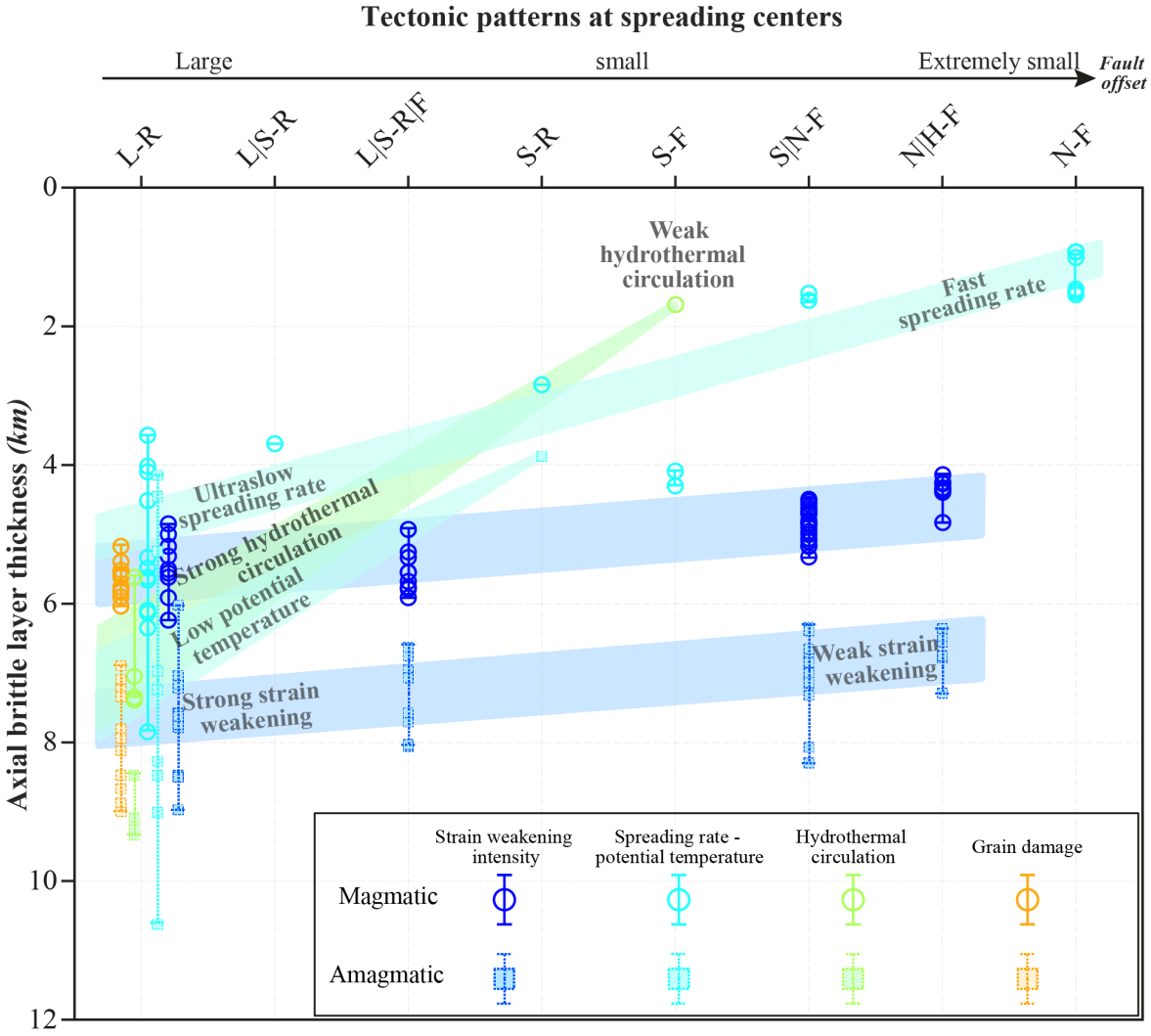

Figure 7. Tectonic patterns versus brittle layer thickness. Circles represent the mean brittle layer thickness at magmatic segments from each model. Dashed

squares mark the mean brittle layer thickness at amagmatic segments from each model. Distributions of brittle layer thickness in different sets of parameters are fitted and presented through colorful areas.

4.2 Why the effect of grain damage is negligible

Using petrological observation and numerical models, Bickert et al., (2020, 2021) systematically investigated the deformation processes of detachment faults and the effects of both grain size reduction and serpentinization. They found that the deformation process of partially serpentinized peridotites is active at the root of detachment fault systems in both brittle and crystal-plastic regions. And that grain size reduction is observed where deviatoric stress is greater than $80 - 270$ Mpa and temperature is larger than 800 ℃. Through thermo-mechanical modelling with these two weakening mechanisms - serpentinization (decreasing cohesion and internal frictional angle at $T < 350$ ℃) and grain size reduction (varying flow law prefactor at $T \sim 800 - 1000$ ℃), they suggested that any single weakening mechanism cannot create flip-flop detachments with reasonable topography. Only by combining both weakening mechanisms, long or short-lived flip-flop detachments could be observed. Compared to their models, self-consistent grain size evolution combing brittle/plastic rheology and ductile rheology with both diffusion and dislocation creep is implemented in our models. We found that grain damage indeed occurs at the root of detachment faults around the brittle-ductile transition and then exhumes with mantle rocks (Figure3-6). However, after a systematic investigation, we find that the effect of grain damage is negligible and may play a subordinate role. This may be related to the following reasons:

1. Grain damage mainly only occurs around brittle-ductile transition where deviatoric stress reaches a peak, strength reduction induced by grain-size sensitive diffusion creep at the root of detachment faults is not sufficient to change the faulting pattern;

2. Although small grain sizes are exhumed along detachment faults, the fault strength is mainly controlled by strain-weakening of friction coefficient rather than grain-size sensitive diffusion creep in the brittle layer;

3. Regardless of the initial grain size, after dynamic equilibration, the grain size tends to be uniform in the partial melting region where the grain growth rate and damage rate are balanced (Figure 5). Accordingly, the viscosity is then relatively uniform and low.

4.3 A set of spreading mechanisms for successive detachment faults

Through the above analysis, here we propose a set of spreading mechanisms to explain the development of successive detachment faults (Figure 8) and compare it with natural observations (Figure 9). Three different types of spreading end-member models are proposed: rolling hinge-coupled model, rolling hinge-decoupled model, and flip-flip model. (1) In the rolling hinge-coupled mode, a very thick axial brittle layer and a strong fault strength reduction lead to very

asymmetric detachment faults and a continuous slip. During the extension of the current fault, strain localization starting from the top of the partial melting region (where the brittle layer is the thinnest) creates a new fault at the footwall which develops listric faults under extension. Meanwhile, the main detachment fault continues to slip and the spreading centers migrate far away from the original position. This may occur at the early stage of magma-poor rifted margins. The axial brittle layer is thick and hydrothermal fluid goes into the mantle along initial high-angle faults to form the serpentinized mantle (Figure 9a), reducing the fault strength and promoting the fault slip. A very asymmetric detachment fault and a series of listric faults form along the magma-poor margin (Gillard et al., 2019; Lymer et al., 2019). With the axial brittle layer thinning, magma upwells and forms a new plate boundary which shows a gradual transition from tectonic-driven to magmatic-driven processes (Gillard, et al., 2017).

Different from the rolling hinge-coupled model, the rolling hinge-decoupled model develops with relatively fixed spreading centers. Owing to the rather thin axial brittle layer, new faults develop into the main detachment fault, resulting in relatively fixed spreading centers. Similar to the deformation jump-decoupled model proposed by Gaillard et al., (2016) based on the observation in the Iberia-Newfound margins, the previously exhumed basement was cut by new detachment faults in the ocean-continent transition region. This model successfully explains the oceanward direction of both the new basement and the new sedimentary sequence (Gillard, et al., 2016).

Consistent with the previous model proposed by Sauter et al., (2013), the flip-flop model successfully explains the development of detachment faults in the Southwest Indian Ridge. Compared with the above two models, according to the earthquake depth and exhumed serpentinized mantle rocks (Cannat et al., 2019), continually thinned axial brittle layer and strong reduction of fault strength lead to polarity change of newly formed fault (Figure 9b), resulting in symmetric spreading centers. In addition, due to the increasing magma supply and the decreasing hydrothermal alternation from amagmatic segment to the fully volcanic magmatic segment, axial brittle thickness decreases, and the fault strength increase. New faults develop a transition from detachment faults to conjugate faults (Figure 9b).

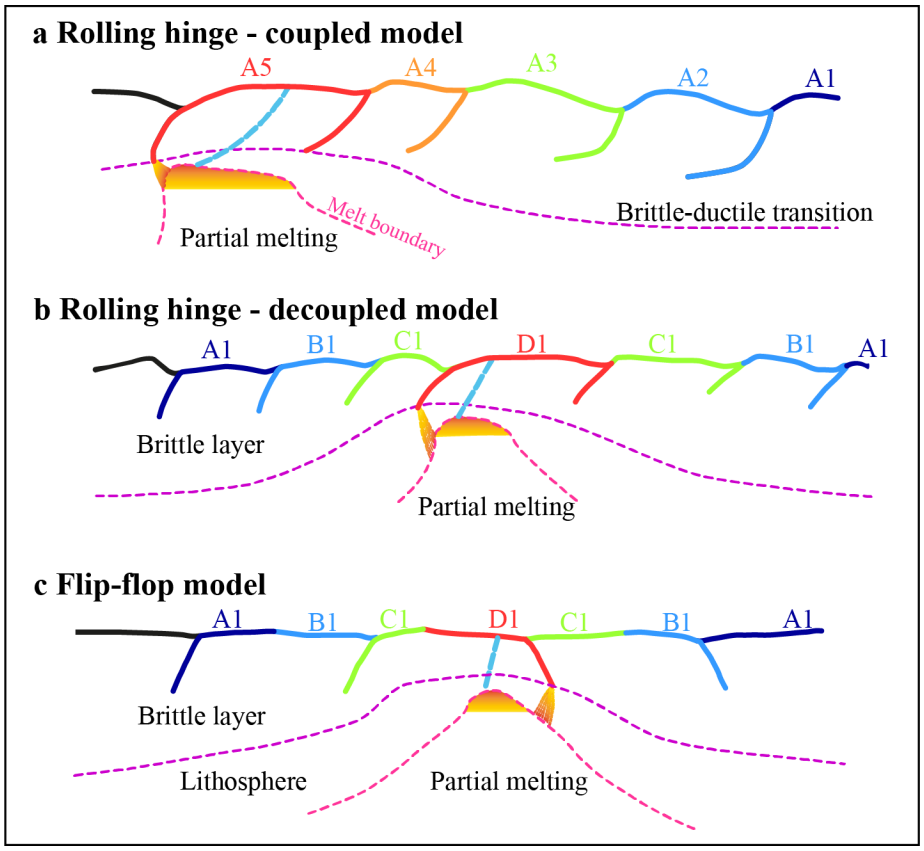

Figure 8. Schematic diagram of three different spreading end-member models along the spreading direction.

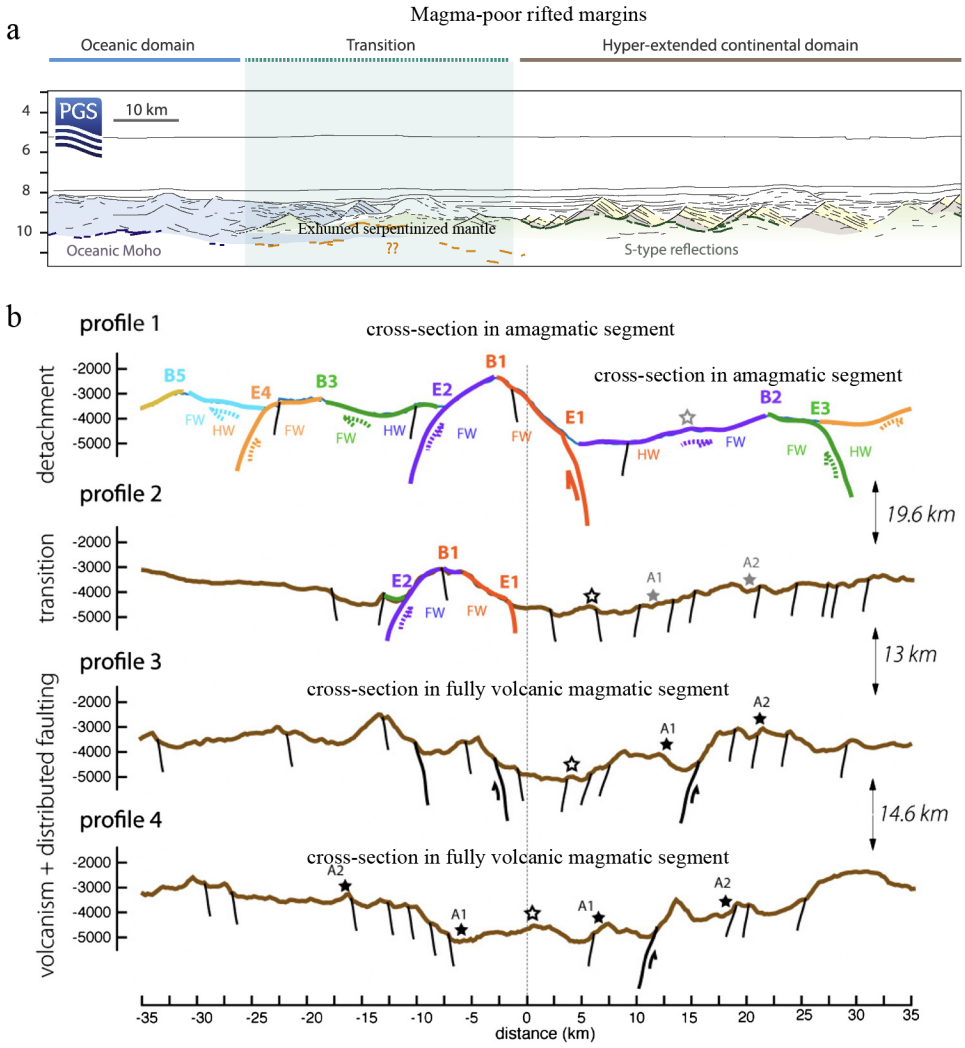

Figure 9. Natural observations. a. Seismic sections from continental to oceanic crusts at magma-poor rifted margins in the Gulf of Guinea (Modified from Gillard et al., 2017, 2019). b. Cross-sections of the region from a nearly amagmatic seafloor (profile 1) to a fully volcanic seafloor (profile 3 and 4) in the 64.6° E at the ultraslow eastern Southwest Indian Ridge.

5 Conclusions

Using 3D magmatic-thermomechanical numerical models, the formation and development of tectonic patterns at spreading centers are thoroughly investigated. To explore the effect of brittle-ductile weakening, both brittle/plastic strain weakening and grain size evolution are fully coupled into the model. A spectrum of tectonic patterns, from asymmetric long-lived detachment faults in

rolling-hinge mode to symmetric conjugate faults in flip-flop mode, are documented in our models, which may provide valuable insights to investigate deformation processes of detachment faults and explore the development of spreading ridges. After systematical numerical results, we found that fault strength reduction and axial brittle layer thickness are two pivotal factors in controlling the faulting patterns and spreading modes. In addition, a set of spreading mechanisms is provided to explain the development of successive detachment faults in variable tectonic settings, which can shed light on better understanding the natural observations.

Strain weakening intensity, which may be induced by localized hydrothermal alteration of faults at spreading centers, plays a significant role in fault strength reduction. Strong strain weakening induces large fault strength reduction, resulting in large fault offset and very asymmetric detachment faults in rolling-hinge mode. When the strain weakening intensity is decreased, the fault strength reduces, resulting in a small fault offset and the transition from short-lived detachment faults to conjugated faults. In addition, grain size reduction is observed at the root of detachment faults, but its effect was found negligible owing to the small fault strength reduction induced by grain damage.

Spreading rate, hydrothermal circulation, and mantle potential temperature strongly impact the brittle layer thickness and the melt supply, which significantly affects the tectonic pattern. Fast spreading rate and weak hydrothermal circulation lead to small heat loss and hot axial thermal configuration with thin axial brittle thickness, resulting in conjugated faults in flip-flop mode. Heat loss plays a crucial role in the axial thermal structure when the spreading rate is low and hydrothermal circulation is enhanced. The resulting increase in the axial brittle layer thickness generates detachment faults transition from flip-flop mode to rolling-hinge mode. Hot mantle potential temperature leads to increased melt supply and disappearance of amagmatic spreading centers.

Acknowledgments

This study is funded by a grant from the China Scholarship Council (201808110216) to M. Liu. Numerical models were run on the Euler cluster from ETH-Zurich. Data analysis and visualization were completed by Matlab and Paraview.

Data Availability Statement

Numerical data used in this study can be obtained in Zendo (https://doi.org/10.5281/zenodo.7018459).

References

Andreani, M., Escartin, J., Delacour, A., Ildefonse, B., Godard, M., Dyment, J., ... & Fouquet, Y. (2014). Tectonic structure, lithology, and hydrothermal signature of the Rainbow massif (Mid-Atlantic Ridge 36° 14 N). Geochemistry, Geophysics, Geosystems, 15(9), 3543-3571.

Bach, W., Garrido, C. J., Paulick, H., Harvey, J., & Rosner, M. (2004). Seawater-peridotite interactions: First insights from ODP Leg 209, MAR 15 N. Geochemistry, Geophysics, Geosystems, 5(9).

Bach, W., Paulick, H., Garrido, C. J., Ildefonse, B., Meurer, W. P., & Humphris, S. E. (2006). Unraveling the sequence of serpentinization reactions: petrography, mineral chemistry, and petrophysics of serpentinites from MAR 15 N (ODP Leg 209, Site 1274). Geophysical research letters, 33(13).

Beard, J. S. et al. (2009). Onset and progression of serpentinization and magnetite formation in olivine-rich troctolite from IODP Hole U1309D. Journal of Petrology, 50(3), 387-403.

Bercovici, D., & Ricard, Y. (2012). Mechanisms for the generation of plate tectonics by two-phase grain-damage and pinning. Physics of the Earth and Planetary Interiors, 202, 27-55.

Bercovici, D., Ricard, Y. (2013). Generation of plate tectonics with two-phase grain-damage and pinning: Source-sink model and toroidal flow. Earth Planet. Sci. Lett. 365, 275–288.

Bercovici, D., Schubert, G., Ricard, Y. (2015). Abrupt tectonics and rapid slab detachment with grain damage. Proceed. National Acad. Sci. 112, 1287-1291.

Bickert, M., Lavier, L., & Cannat, M. (2020). How do detachment faults form at ultraslow mid-ocean ridges in a thick axial lithosphere?. Earth and Planetary Science Letters, 533, 116048.

Bickert, M., Cannat, M., Tommasi, A., Jammes, S., & Lavier, L. (2021). Strain localization in the root of detachment faults at a melt-starved mid-ocean ridge: a microstructural study of abyssal peridotites from the Southwest Indian Ridge. Geochemistry, Geophysics, Geosystems, 22(5), e2020GC009434.

Boschi, C., Früh-Green, G. L., Delacour, A., Karson, J. A., & Kelley, D. S. (2006). Mass transfer and fluid flow during detachment faulting and development of an oceanic core complex, Atlantis Massif (MAR 30 N). Geochemistry, Geophysics, Geosystems, 7(1).

Boschi, C., Bonatti, E., Ligi, M., et al. (2013). Serpentinization of mantle peridotites along an uplifted lithospheric section, Mid Atlantic Ridge at 11 N. Lithos, 178, 3-23.

Buck, W. R. (1988). Flexural rotation of normal faults. Tectonics, 7(5), 959-973.

Buck, W. R., Lavier, L. L., & Poliakov, A. N. (2005). Modes of faulting at mid-ocean ridges. Nature, 434(7034), 719-723.

Cannat, M., Sauter, D., Lavier, L., Bickert, M., Momoh, E., & Leroy, S. (2019). On spreading modes and magma supply at slow and ultraslow mid-ocean ridges. Earth and Planetary Science Letters, 519, 223-233.

Chen, Y., & Morgan, W. J. (1990). A nonlinear rheology model for mid-ocean ridge axis topography. Journal of Geophysical Research: Solid Earth, 95(B11), 17583-17604.

Clauser, C., Huenges, E. (1995). Thermal conductivity of rocks and minerals. In: Ahrens, T.J. (editor), Rock Physics and Phase Relations. AGU Reference Shelf 3. American Geophysical Union, Washington DC, pp. 105–126.

Coogan, L. A., Kasemann, S. A., & Chakraborty, S. (2005). Rates of hydrothermal cooling of new oceanic upper crust derived from lithium-geospeedometry. Earth and Planetary Science Letters, 240(2), 415-424.

Escartín, J., Hirth, G., & Evans, B. (2001). Strength of slightly serpentinized peridotites: Implications for the tectonics of oceanic lithosphere. Geology, 29(11), 1023-1026.

Escartín, J., Smith, D. K., Cann, J., Schouten, H., Langmuir, C. H., & Escrig, S. (2008). Central role of detachment faults in accretion of slow-spreading oceanic lithosphere. Nature, 455(7214), 790-794.

deMartin, B. J., Sohn, R. A., Pablo Canales, J., & Humphris, S. E. (2007). Kinematics and geometry of active detachment faulting beneath the Trans-Atlantic Geotraverse (TAG) hydrothermal field on the Mid-Atlantic Ridge. Geology, 35(8), 711-714.

Gerya, T. V. (2013). Three-dimensional thermomechanical modeling of oceanic spreading initiation and evolution. Physics of the Earth and Planetary Interiors, 214, 35-52.

Gerya, T. V., & Meilick, F. I. (2011). Geodynamic regimes of subduction under an active margin: effects of rheological weakening by fluids and melts. Journal of Metamorphic Geology, 29(1), 7-31.

Gillard, M., Manatschal, G., & Autin, J. (2016). How can asymmetric detachment faults generate symmetric Ocean Continent Transitions?. Terra Nova, 28(1), 27-34.

Gillard, M., Sauter, D., Tugend, J., Tomasi, S., Epin, M. E., & Manatschal, G. (2017). Birth of an oceanic spreading center at a magma-poor rift system. Scientific Reports, 7(1), 1-6.

Gillard, M., Tugend, J., Müntener, O., Manatschal, G., Karner, G. D., Autin, J., ... & Ulrich, M. (2019). The role of serpentinization and magmatism in the formation of decoupling interfaces at magma-poor rifted margins. Earth-Science Reviews, 196, 102882.

Grevemeyer, I., Reston, T. J., & Moeller, S. (2013). Microseismicity of the Mid-Atlantic Ridge at 7° S–8° 15 S and at the Logatchev Massif oceanic core complex at 14° 40 N–14° 50 N. Geochemistry, Geophysics, Geosystems, 14(9), 3532-3554.

Harding, J. L., Van Avendonk, H. J., Hayman, N. W., Grevemeyer, I., Peirce, C., & Dannowski, A. (2017). Magmatic-tectonic conditions for hydrothermal venting on an ultraslow-spread oceanic core complex. Geology, 45(9), 839-842.

Hilairet, N., B. et al. (2007). High-pressure creep of serpentine, interseismic deformation, and initiation of subduction. Science, 318, 1910–1913.

Hirth, G., Kohlstedt, D. (2003). Rheology of the upper mantle and the mantle wedge: a view from the experimentalists. In: Eiler, J. (Ed.), Subduction Factor Monograph, vol.138. American Geophysical Union,Washington, DC, pp. 83–105.

Hofmeister, A. M. (1999). Mantle values of thermal conductivity and the geotherm from Phonon lifetimes. Science, 283, 1699–1706.

Huismans, R. S., & Beaumont, C. (2002). Asymmetric lithospheric extension: The role of frictional plastic strain softening inferred from numerical experiments. Geology, 30(3), 211-214.

Huismans, R. S., & Beaumont, C. (2003). Symmetric and asymmetric lithospheric extension: Relative effects of frictional-plastic and viscous strain softening. Journal of Geophysical Research: Solid Earth, 108(B10).

Karato, S., Wu, P. (1993) Rheology of the upper mantle: a synthesis. Science 260, 771–778.

Klein, F., Bach, W., Jöns, N., McCollom, T., Moskowitz, B., & Berquó, T. (2009). Iron partitioning and hydrogen generation during serpentinization of abyssal peridotites from 15 N on the Mid-Atlantic Ridge. Geochimica et Cosmochimica Acta, 73(22), 6868-6893.

Lavier, L. L., Roger Buck, W., & Poliakov, A. N. (1999). Self-consistent rolling-hinge model for the evolution of large-offset low-angle normal faults. Geology, 27(12), 1127-1130.

Liu, M., Gerya, T., & Rozel, A. B. (2022). Self-organization of magma supply controls crustal thickness variation and tectonic pattern along melt-poor mid-ocean ridges. Earth and Planetary Science Letters, 584, 117482.

Lymer, G., Cresswell, D. J., Reston, T. J., Bull, J. M., Sawyer, D. S., Morgan, J. K., ... & Shillington, D. J. (2019). 3D development of detachment faulting during continental breakup. Earth and Planetary Science Letters, 515, 90-99.

MacLeod, C. J., Escartin, J., Banerji, D., Banks, G. J., Gleeson, M., Irving, D. H. B., ... & Smith, D. K. (2002). Direct geological evidence for oceanic detachment faulting: The Mid-Atlantic Ridge, 15 45 N. Geology, 30(10), 879-882.

MacLeod, C. J., Carlut, J., Escartín, J., Horen, H., & Morris, A. (2011). Quantitative constraint on footwall rotations at the 15° 45 N oceanic core complex, Mid-Atlantic Ridge: Implications for oceanic detachment fault processes. Geochemistry, Geophysics, Geosystems, 12(5).

Maffione, M., Morris, A., Plümper, O., & van Hinsbergen, D. J. (2014). Magnetic properties of variably serpentinized peridotites and their implication for the evolution of oceanic core complexes. Geochemistry, Geophysics, Geosystems, 15(4), 923-944.

Mével, C. (2003). Serpentinization of abyssal peridotites at mid-ocean ridges. Comptes Rendus Geoscience, 335(10-11), 825-852.

Morgan, J. P., & Chen, Y. J. (1993). The genesis of oceanic crust: Magma injection, hydrothermal circulation, and crustal flow. Journal of Geophysical Research: Solid Earth, 98(B4), 6283-6297.

Mulyukova, E., Bercovici, D. (2017). Formation of lithospheric shear zones: Effect of temperature on two-phase grain damage. Phys. Earth Planet. Inter. 270, 195–212.

Olive, J. A., Behn, M. D., & Tucholke, B. E. (2010). The structure of oceanic core complexes controlled by the depth distribution of magma emplacement. Nature Geoscience, 3(7), 491-495.

Olive, J. A., & Dublanchet, P. (2020). Controls on the magmatic fraction of extension at mid-ocean ridges. Earth and Planetary Science Letters, 549, 116541.

Paterson, M. S., & Wong, T. F. (2005). Experimental rock deformation-the brittle field. Springer Science & Business Media.

Plümper, O., Røyne, A., Magrasó, A., & Jamtveit, B. (2012). The interface-scale mechanism of reaction-induced fracturing during serpentinization. Geology, 40(12), 1103-1106.

Plümper, O., Beinlich, A., Bach, W., Janots, E., & Austrheim, H. (2014). Garnets within geode-like serpentinite veins: Implications for element transport, hydrogen production and life-supporting environment formation. Geochimica et Cosmochimica Acta, 141, 454-471.

Poirier, J. P. (1980). Shear localization and shear instability in materials in the ductile field. Journal of Structural Geology, 2(1-2), 135-142.

Ranalli, G. Rheology of the Earth (Chapman and Hall, 1995).

Rozel, A., Ricard, Y., & Bercovici, D. (2011). A thermodynamically self-consistent damage equation for grain size evolution during dynamic recrystallization. Geophysical Journal International, 184(2), 719-728.

Sauter, D., Cannat, M., Rouméjon, S., et al. (2013). Continuous exhumation of mantle-derived rocks at the Southwest Indian Ridge for 11 million years. Nature Geoscience, 6(4), 314-320.

Schierjott, J. C., Thielmann, M., Rozel, A. B., Golabek, G. J., Gerya, T. V. (2020). Can Grain Size Reduction Initiate Transform Faults? —Insights From a 3-D Numerical study. Tectonics, 39(10), e2019TC005793.

Schroeder, T., John, B., & Frost, B. R. (2002). Geologic implications of seawater circulation through peridotite exposed at slow-spreading mid-ocean ridges. Geology, 30(4), 367-370.

Sibrant, A. L. R., Mittelstaedt, E., Davaille, A., Pauchard, L., Aubertin, A., Auffray, L., & Pidoux, R. (2018). Accretion mode of oceanic ridges governed by axial mechanical strength. Nature Geoscience, 11(4), 274-279.

Tao, C., Seyfried, W. E. et al. (2020). Deep high-temperature hydrothermal circulation in a detachment faulting system on the ultra-slow spreading ridge. Nature Communications, 11(1), 1-9.

Turcotte, D. L. & Schubert, G. Geodynamics (Cambridge Univ. Press, 2002).

van der Zwan, F. M. et al. (2017). Lower crustal hydrothermal circulation at slow-spreading ridges: evidence from chlorine in Arctic and South Atlantic basalt glasses and melt inclusions. Contributions to Mineralogy and Petrology, 172(11), 1-23.

Vissers, R. L. M., Drury, M. R., Hoogerduijn, E. H., Spiers, C. J., & Van der Wal, D. (1995). Mantle shear zones and their effect on lithosphere strength during continental breakup. Tectonophysics, 249(3-4), 155-171.

Zhou, F., Dyment, J., Tao, C., & Wu, T. (2022). Magmatism at oceanic core complexes on the ultraslow Southwest Indian Ridge: Insights from near-seafloor magnetics. Geology, 50(6), 726-730